

ESTABLISHMENT AND APPLICATION OF HEAT FLOW COUPLING MODEL

by

**Jun HE^a, Gao-Liang PENG^a, Ling-Tao YU^{b,a*}, Chen-Zheng LI^{b,a},
Chuan-Hao LI^a, and Guo-Juan CHENG^a**

^a School of Mechanics and Electronics, Harbin Institute of Technology, Harbin, China

^b College of Mechanical and Electrical Engineering, Harbin Engineering University, Harbin, China

Original scientific paper

<https://doi.org/10.2298/TSCI160422025P>

Wax deposition on walls of oil pipes is a common occurrence in crude oil extraction and is one of the major impediments to oilfield production. The most common method of paraffin removal is superconducting car thermal washing. This study proposes a heat flow coupling model that can analyze the temperature of the tubing-casing annular space to solve the low efficiency problem caused by adjusting initial parameters empirically. Using the superconducting car thermal washing process at the test oil well in city of Daqing, China as research object, the real-time temperature of annulus under various initial conditions is acquired by the fully-distributed Raman optical fiber temperature monitoring system. Compared with the real time data, theoretical data has a maximum deviation of 5 °C, this result verifies the accuracy of the model. Based on the model, the study investigates the optimal initial parameters of superconducting car thermal washing by taking effective depth as an optimization goal. The optimal parameters for oil wells with different working conditions are obtained to improve the effectiveness of paraffin removal and increase thermal efficiency. This study provides theoretical support and an inspection method to promote superconducting car thermal washing and paraffin removal as well as to improve productive efficiency.

Key words: *superconducting car thermal washing, heat flow coupling model, optimal initial parameters, effective depth*

Introduction

During crude oil extraction, wax dissolved in petroleum tends to be deposited on the inner walls of oil pipes, sucker rods, pumps, and so on, because of the influence of temperature difference between the oil and the pipe wall, decrease of pressure, and components' compositional and structural analysis of crude oils. As the wax accumulates, the walls of oil pipes gradually thicken and the pipe diameter decreases. This gradual constriction leads to a decline in pump efficiency, impedes oil extraction, and finally reduces oil production. Therefore, removing this wax periodically is necessary [1, 2].

The commonly used techniques of paraffin removal include technology using strong magnetic force, microorganisms, chemicals, mechanical methods, and thermal paraffin removal techniques [3-6]. The paraffin deposition problem can also be solved by heating cable application, which can melt the paraffin by heating a steel pipe with a cable [7]. The present study

* Corresponding author, e-mail: yulingtao2016@gmail.com

focuses on the superconducting car thermal wash. Its process is as follows. Thermal wash liquid is heated by a heating device driven by natural gas or liquid gas and is then injected into a tubing-casing annular space to warm the oil well. Then, the thermal wash liquid is extracted by the pump through the oil pipes and goes back to the heating device, where the thermal wash liquid prepares to go for the next loop.

Based on the practical experience of workers, inlet liquid temperature, liquid injection rate, liquid extraction rate, and cost of time are the four main factors that can influence the effectiveness of thermal wash. These parameters are usually manually adjusted by experienced workers. But the parameters can be also adjusted theoretically based on the temperature distribution of the annulus.

Foreign researchers have conducted significant studies on the temperature distribution of the annulus. Focusing on well drilling and completion, one study developed a unified approach to model heat transfer in various situations, which results in physically sound solutions for many routine production operation problems [8]. Another study focuses on transient liquid in wellbore or reservoir systems and presents a transient wellbore model coupled with a semi-analytic temperature model to compute a wellbore-fluid-temperature profile in flowing and shut-in wells [9]. Although these studies analyze the temperature distribution of the annulus in different situations, they are computationally expensive and not very generic.

This study proposes a heat flow coupling model that can theoretically analyze the temperature of the tubing-casing annular space to solve the low efficiency problem caused by empirically adjusting initial parameters of thermal washing. The study is based on the superconducting car thermal washing process performed at the test oil well in Daqing. The real-time temperature of annulus under different initial conditions was obtained by a fully-distributed Raman optical fiber temperature monitoring system. The theoretical data and experimental data are compared to verify the heat flow coupling model. Based on the model, this study investigates the influence of initial parameters on the effective depth at the test oil well and determines the optimal initial parameters with the effective depth as optimization objective. The optimal initial parameters are applied to the oil well to improve the thermal efficiency, and ultimately increase oil production and productive efficiency.

Establishment of heat flow coupling model

When thermal washing liquid is injected into the tubing-casing annular space and moves downward along the shaft, the heat carried by the thermal washing liquid spreads inward and outward from the annulus because of the radial temperature difference. The heat is transferred inward to the liquid in the oil pipe and outward to the casing pipe by way of heat conduction, so it cools down continuously during downward movement, which causes a drop in axial temperature.

When the thermal washing liquid returns to the ground because of the oil well pump, the thermal washing liquid in the annulus transfers heat to thermal washing liquid in the oil pipe under the drive of radial temperature difference. Therefore, the thermal washing liquid in the oil pipe heats up ceaselessly during its upward movement.

Before the model is established, the following hypotheses are made:

- Infinitesimal body length, dl , of the selected thermal washing liquid is short, and the temperature of this infinitesimal body can be approximately calculated as the inlet temperature of the infinitesimal body.
- The area of the stratum is so big that the increase of temperature is small. Thus, the stratum is assumed to be a body of constant temperature.

- Based on the assumption that the casing pipe and cement sheath are combined as the medium for the thermal washing liquid in the annulus to transfer heat outward, the heat conductivity coefficient of this medium is $k_w = 5 \text{ W/m}^\circ\text{C}$.

The washing liquid used in practice is a mixture of oil and water. Therefore, the density and specific heat capacity of the mixture need to be calculated. The parameters are shown in tab. 1.

Table 1. Components of the mixture of oil and water

| | Density [kgm ⁻³] | Volume ratio [%] | Specific heat capacity [Jkg ⁻¹ °C ⁻¹] |
|-------|------------------------------|------------------|--|
| Water | 1 | 98 | 4235 |
| Oil | 0.85 | 2 | 2500 |

The density of the oil-water mixture $\rho = 0.997 \text{ kg/m}^3$, and its specific heat capacity $c = 4205 \text{ J/kg}^\circ\text{C}$.

In an actual oil field, different oil wells adopt different kinds of steel for oil pipes and casing pipes. Commonly used types of steel are J55, N80, and P110 whose sizes of oil pipes and casing pipes are shown in tab. 2. Heat flow coupling models will be established to help guide the practical thermal washing process.

Table 2. Sizes of oil pipes and casing pipes of materials

| | Casing pipes | | Oil pipes | |
|------|------------------------|---------------------|------------------------|---------------------|
| | External diameter [mm] | Wall thickness [mm] | External diameter [mm] | Wall thickness [mm] |
| J55 | 139.7 | 6.2 | 89 | 7.17 |
| N80 | 139.7 | 7.72 | 89 | 7.17 |
| P110 | 139.7 | 10.54 | 89 | 7.17 |

Establishment of heat flow coupling model in tubing-casing annular space

At the depth of $(n-1)dl$ from the wellhead in the annulus, the infinitesimal body of thermal washing liquid with a length of dl is selected and its energy diagram is shown in fig. 1.

According to energy conservation law, the heat $Q_{pa}[(n-1)dl]$ transferred into the infinitesimal body along the axial direction is equal to the sum of the heat $Q_{pa}(ndl)$ transferred from the infinitesimal body along the axial direction, the heat $Q_{r1}[(n-1)dl]$ scattering along the inner radial direction in the infinitesimal body, and the heat $Q_{r2}[(n-1)dl]$ scattering along the outer radial direction, as expressed in the following:

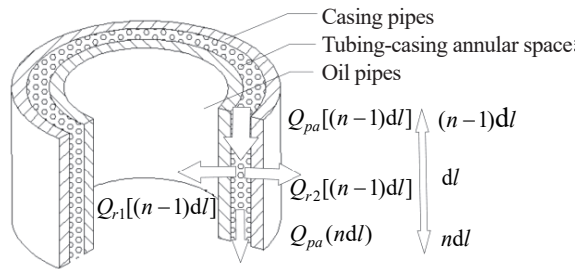


Figure 1. Energy diagram for infinitesimal body of thermal washing liquid in tubing-casing annular space

$$Q_{pa}[(n-1)dl] - Q_{pa}(ndl) = Q_{r1}[(n-1)dl] + Q_{r2}[(n-1)dl] \quad (1)$$

Based on the heat conduction flow formula of a 1-D cylindrical wall:

$$Q = \frac{2\pi kl(t_1 - t_2)}{\ln \frac{r_2}{r_1}} \quad (2)$$

where k [$\text{Wm}^{-1}\text{C}^{-1}$] is the heat conductivity coefficient of cylindrical wall, l [m] – the length of cylindrical wall, t_1 [$^{\circ}\text{C}$] – the inside temperature of cylindrical wall, t_2 [$^{\circ}\text{C}$] – the lateral temperature of cylindrical wall, r_1 [m] – the inner radius of cylindrical wall, and r_2 [m] – the external radius of cylindrical wall.

The energy of various parts of the annulus is obtained:

$$Q_{pa}[(n-1)dl] = m_a c T_{\alpha(n-1)} \quad (3)$$

$$Q_{pa}(ndl) = m_a c T_{\alpha n} \quad (4)$$

$$Q_{r1}[(n-1)dl] = \int \frac{2\pi k_t dl [T_{a(n-1)} - T_{t(n-1)}]}{\ln \frac{r_{to}}{r_{ti}}} dt \quad (5)$$

$$Q_{r2}[(n-1)dl] = \int \frac{2\pi k_w dl [T_{a(n-1)} - T_{s(n-1)}]}{\ln \frac{r_s}{r_{ci}}} dt \quad (6)$$

where m_a [kg] is the mass of infinitesimal body (determined by external radius of oil pipe r_{to} [m], inner radius of casing pipe r_{ci} [m], thermal washing liquid density ρ [kgm^{-3}], and dl [m]), $T_{\alpha(n-1)}$ [$^{\circ}\text{C}$] – the inlet temperature of infinitesimal body in the annulus, $T_{\alpha n}$ [$^{\circ}\text{C}$] – the outlet temperature of infinitesimal body in the annulus, k_t [$\text{Wm}^{-1}\text{C}^{-1}$] – the heat conductivity coefficient of oil pipe, r_{ti} [m] – the inner radius of oil pipe, r_s [m] – the external radius of cement sheath, $T_{t(n-1)}$ [$^{\circ}\text{C}$] – the temperature of infinitesimal body in oil pipe at a depth of $(n-1)dl$ from the wellhead, $T_{s(n-1)}$ [$^{\circ}\text{C}$] – the temperature of stratum at a depth of $(n-1)dl$ from the wellhead, and

$$T_{s(n-1)} = \begin{cases} l, & n \leq \frac{h}{dl} \\ T_0 + \lambda(n-1)dl, & \frac{h}{dl} < n \leq \frac{H}{dl} \end{cases}$$

where l [$^{\circ}\text{C}$] is the temperature near earth's surface, h – the depth from earth's surface (determined by the measured formation temperature curve), T_0 [$^{\circ}\text{C}$] – the initial temperature of earth's surface, λ [$^{\circ}\text{Cm}^{-1}$] – the temperature gradient of stratum, and H – the maximum depth of the oil wells from earth's surface.

The iteration expression of the outlet temperature of the infinitesimal body in the annulus can be obtained:

$$T_{\alpha n} = T_{\alpha(n-1)} - \frac{2\pi k_t dl [T_{a(n-1)} - T_{t(n-1)}] dl}{m_a c \ln \frac{r_{to}}{r_{ti}} v_i} - \frac{2\pi k_w dl [T_{a(n-1)} - T_{s(n-1)}] dl}{m_a c \ln \frac{r_s}{r_{ci}} v_i}, \quad n = 1, 2, \dots, \frac{H}{dl} \quad (7)$$

where liquid injection speed $v_\varepsilon = q_\varepsilon / s_\varepsilon$, and s_ε is the cross-sectional area of the annulus.

In eq. (7), initial conditions are: $T_{\alpha 0}$ is the inlet temperature of thermal washing liquid, and the temperature of the thermal washing liquid in the oil pipe is equal to the stratum temperature at the first cycle.

Establishment of heat flow coupling model in oil pipe

At the depth of $(n-1)dl$ from the wellhead in the oil pipe, the infinitesimal body of thermal washing liquid with a length of dl is selected and its energy diagram is shown in fig. 2. According to energy conservation law, the sum of the heat $Q_{pt}(ndl)$ transferred into the infinitesimal body along the axial direction and the heat $Q_r(ndl)$ transferred into the infinitesimal body along the radial direction is equal to the heat $Q_{pt}[(n-1)dl]$ transferred from the infinitesimal body along the axial direction, as expressed:

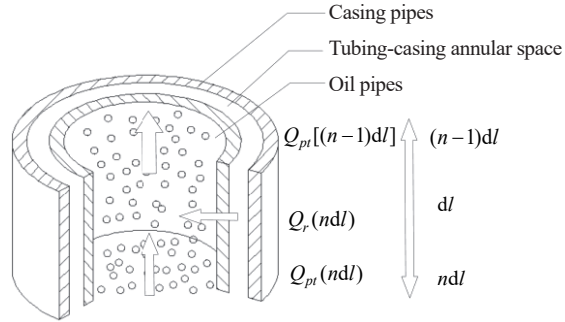


Figure 2. Energy diagram for infinitesimal body of thermal washing liquid in oil pipe

$$Q_{pt}(ndl) + Q_r(ndl) = Q_{pt}[(n-1)dl] \tag{8}$$

The energy of various parts is described:

$$Q_{pt}(ndl) = m_t c T_m \tag{9}$$

$$Q_{pt}[(n-1)dl] = m_t c T_{t(n-1)} \tag{10}$$

$$Q_r(ndl) = \int \frac{2\pi k_t dl (T_{an} - T_m)}{\ln \frac{r_{to}}{r_{ti}}} dt \tag{11}$$

where m_t [kg] is the mass of infinitesimal body of thermal washing liquid in oil pipe (determined by inner radius of oil pipe r_{ti} [m], thermal washing liquid density ρ [kgm^{-3}], and dl [m]), and T_m [$^{\circ}\text{C}$] – the inlet temperature of infinitesimal body of thermal washing liquid in oil pipe.

The iteration expression of the outlet temperature of the infinitesimal body in the oil pipe can be obtained:

$$T_{t(n-1)} = T_m + \frac{2\pi k_t dl (T_{an} - T_m)}{m_t c \ln \frac{r_{to}}{r_{ti}} \frac{dl}{v_e}}, \quad n = \frac{H}{dl}, \quad \frac{H}{dl} - 1, \dots, 1 \tag{12}$$

where liquid extraction speed $v_e = q_e / s_e$ and s_e is the cross-sectional area of the oil pipe.

The initial conditions in eq. (12) are as follows: $T_m = T_{an}$ is the temperature of the thermal washing liquid at the depth of H , and $T_{an} \sim T_{a1}$ is obtained via eq. (7).

Iterative calculation is performed for eq. (12) via MATLAB. Until now, the infinitesimal body completes a cycle from the entrance of the tubing-casing annular space to the exit of the oil pipe. The temperature distribution along the axial direction in the oil pipe and tubing-casing annular space can be obtained for the first cycle.

When the second cycle, $m = 2$, starts, $T_{s0}, T_{s1}, \dots, T_{s(n-1)}$ remains unchanged, and $T_{t0}, T_{t1}, \dots, T_{t(n-1)}$ is obtained according to eq. (12) as a known condition for the solution of eq. (7). Such loop up to the end, the temperature distribution of the thermal washing liquid along the axial direction in the oil pipe and annulus after thermal washing can be obtained.

Determination of time in heat flow coupling model

To determine the time of heat flow coupling model, the time required for one loop must first be calculated, this time is also the time required for the infinitesimal body to travel from the entrance of the annulus to the exit of the oil pipe. First, the following assumptions are made.

- Because of the larger injection flow amount per unit of time, the infinitesimal body only takes a very short time to travel from the entrance of the annulus to the dynamic liquid level. Thus, this period is neglected in the calculation.
- The distances between the dynamic liquid level and the pump vary in different oil wells. In the present study, this distance is set to 50 m.

The total volume under the dynamic liquid level and in the oil pipe:

$$V = \pi r_{ci}^2 H + \pi (r_{ci}^2 - r_{io}^2) 50 \quad (13)$$

The time of the heat flow coupling model:

$$t = \frac{q_\varepsilon}{V} \quad (14)$$

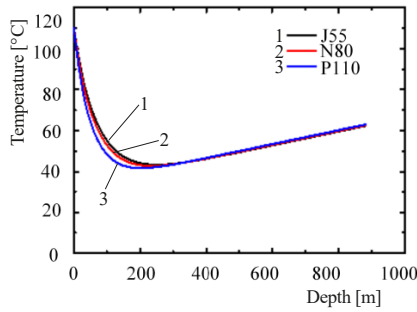


Figure 3. Results of heat flow coupling model in three kinds of materials

Heat flow coupling analysis is performed on the superconducting car thermal washing in three experimental wells whose materials of oil pipes and casing pipes are J55, N80, P110. The parameters in wells (the sizes of oil pipes and casing pipes shown in tab. 2) are: $dl = 0.5$ m, $r_s = 115$ mm, $T_{\alpha 0} = 110$ °C, $v_i = 1.94$ m/s, $v_\varepsilon = 0.124$ m/s, $c = 4205$ J/kg°C, $H = 880$ m, $k_w = 5$ W/m°C, $k_t = 18.5$ W/m°C, $\rho = 0.997 \cdot 10^3$ kg/m³, $T_0 = 35$ °C, $\lambda = 0.034$ °C/m, $t_{J55} = 3.15$ h, $t_{N80} = 3.13$ h, and $t_{P110} = 3.10$ h. Results of the calculation are shown in fig. 3. The actual production can be optimized according to these curves.

Application of heat flow coupling model in superconducting car thermal washing

Establishment of Raman optical fiber temperature monitoring system

Demodulation of Raman optical fiber sensor

Common demodulation methods for Raman optical fiber sensor are anti-Stokes scattering demodulation method, anti-Stokes and Stokes scattering ratio demodulation method, and anti-Stokes and Rayleigh scattering ratio demodulation method, and their expressions are listed, respectively, [10]:

$$\frac{N_{AS}(T)}{N_{AS}(T_0)} = \frac{\exp\left(\frac{h\Delta\nu}{\kappa T_0}\right) - 1}{\exp\left(\frac{h\Delta\nu}{\kappa T}\right) - 1} \quad (15)$$

$$\frac{\frac{N_{AS}(T)}{N_s(T)}}{\frac{N_{AS}(T_0)}{N_s(T_0)}} = \frac{\exp\left(\frac{-h\Delta\nu}{\kappa T}\right)}{\exp\left(\frac{-h\Delta\nu}{\kappa T_0}\right)} \quad (16)$$

$$\frac{\frac{N_{AS}(T)}{N_R(T)}}{\frac{N_{AS}(T_0)}{N_R(T_0)}} = \frac{\exp\left(\frac{-h\Delta\nu}{\kappa T_0}\right) - 1}{\exp\left(\frac{-h\Delta\nu}{\kappa T}\right) - 1} \quad (17)$$

where N_s is the Stokes Raman scattering photon number, N_{AS} – anti-Stokes Raman scattering photon number, N_R – Rayleigh scattering photon number, $\Delta\nu$ – Raman phonon frequency, h – Planck constant, and κ – Boltzmann constant.

The frequency distribution of the optical fiber scattering shows that the light intensity of anti-Stokes scattering and Stokes scattering is substantially in the same order of magnitude. Moreover, anti-Stokes and Stokes scattering ratio demodulation method can not only demodulate temperature signal, but can also eliminate the effects of intrinsic loss and unevenness in optical fiber. Temperature measurement accuracy can be improved, so the demodulation of Raman optical fiber sensor uses the anti-Stokes and Stokes scattering ratio demodulation method.

Structure design of Raman optical fiber sensor [11, 12]

The optical fiber itself is fragile and easily broken, and the environment under the oil well is highly complex. Thus, the optical fiber needs to be encapsulated before it is placed on the outer surface of the oil pipes to monitor temperature. The preliminary design of the encapsulation is shown in fig. 4. The outside heat needs to travel through a variety of materials to reach the optical fiber after it is encapsulated. Thus, the sheath need to have the attributes that can protect the optical fiber and also transfer heat quickly. The PE sheath, PU sheath, and ring oxygen sheath are selected at first, and then the multi-interface heat conduction rates of the temperature of these three materials are analyzed to judge if their temperature sensitivities meet the requirements.

To analyze the multi-interface heat conduction rate of temperature, the structure of encapsulation must be simplified to a double homogeneous cylindrical wall model, as shown in fig. 5.

The heat transfer rate of the cylindrical wall is:

$$q = -k_a 2\pi r L \frac{\partial T}{\partial r} \quad (18)$$

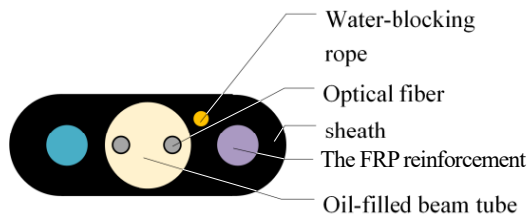


Figure 4. Encapsulation structure of sensor

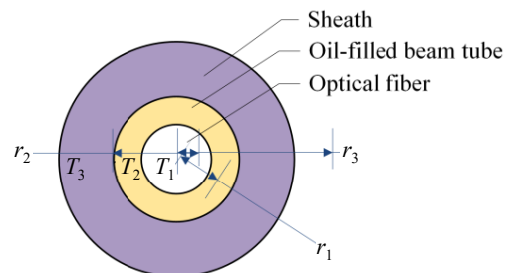


Figure 5. Simplified diagram of encapsulation structure

so the relationship between the inside and outside temperature of the double cylindrical wall can be calculated by eq. (19):

$$T_3 = T_1 - \frac{q_1}{2\pi k_a L} \ln \frac{r_2}{r_1} - \frac{q_2}{2\pi k_b L} \ln \frac{r_3}{r_2} \quad (19)$$

Thus, the heat transfer rate of the double cylindrical wall can be obtained:

$$q = \frac{2\pi L(T_1 - T_3)}{\left(\frac{1}{k_a}\right) \ln\left(\frac{r_2}{r_1}\right) + \left(\frac{1}{k_b}\right) \ln\left(\frac{r_3}{r_2}\right)} \quad (20)$$

where L [m] is the length of the cylinders, k_a [$\text{Wm}^{-1}\text{C}^{-1}$] – the heat conductivity coefficient of the oil-filled beam tube, k_b [$\text{Wm}^{-1}\text{C}^{-1}$] – heat conductivity coefficient of the sheath, r_1 [m] – the internal radius of the oil-filled beam tube, r_2 [m] – the external radius of the oil-filled beam tube, r_3 [m] – the external radius of the sheath, T_1 [$^{\circ}\text{C}$] – the temperature measured by the optical fiber, and T_3 [$^{\circ}\text{C}$] – actual temperature of the thermal washing liquid in the tubing-casing annular space.

Equation (20) shows that the heat transfer rate is related to the heat conductivity coefficient and the radius of the oil-filled beam tube and the sheath. Table 3 shows the heat conductivity coefficient of the PE sheath, PU sheath, and ring oxygen sheath.

Table 3. Heat conductivity coefficient of materials

| Material | PE sheath | PU sheath | Ring oxygen sheath |
|---|-----------|-----------|--------------------|
| The heat conductivity coefficient [$\text{Wm}^{-1}\text{K}^{-1}$] | 0.4 | 0.027 | 0.2 |

From eq. (20), when the radius of the oil-filled beam tube and sheath remains unchanged, the PE sheath can ensure high heat transfer rate. The PE sheath has enough temperature sensitivity and is suitable to monitor the temperature of the tubing-casing annular space.

The preceding analysis settles the encapsulation method of the sensor. Next, the protection and positioning design is developed. The sensor needs to be protected from the side pressure. In addition, the sensor and the axis of the oil pipe need to be parallel to each other, and this position must be secured to properly achieve distributed temperature monitoring. Side pressure protection can be achieved by using high-strength stainless steel in the coupling position of the oil pipes. Secure positioning can be achieved by using a clamping process to ensure that circumferential position is fixed in the coupling position of oil pipes and by fixing the sensor position using a fixing clamp in the middle of the oil pipes. This protection and positioning design ensures the accuracy of the distributed temperature monitoring system.

The Raman optical fiber sensors need to be calibrated before they are used in the temperature monitoring of the annulus. Based on the experiments, the sensitivity coefficient remains stable. It does not vary with temperature changes and does not vary with distance changes.

Finally, the Raman optical fiber sensor is fixed on the outer surface of the oil pipes to monitor the temperatures of the tubing-casing annular space during oil-field heat washover, fig. 6, shows the schematic of this temperature monitoring system.

Data acquisition and analysis of superconducting car thermal washing

The distribution of temperature in thermal washing process can be collected at different times by the Raman optical fiber temperature monitoring system to observe the

change of effective depth during superconducting car thermal washing at a certain test well at Daqing Field.

The temperature of the oil well can be monitored before oil-field heat washover to determine the distribution of temperature in stratum, as shown in fig. 7. The temperature has a linear growth trend. The influence of atmospheric temperature on the near-surface Stratigraphic section is obvious. Moreover, because the optical fibers need to be connected with the demodulator, about 10 meters of optical fiber are above the ground. These two reasons explain why the temperature on the near-surface Stratigraphic section is essentially unchanged; with the increase of depth, the stratum temperature grows approximately linearly.

The expression of stratum temperature in the test well is:

$$T_{s(n-1)} = \begin{cases} 30, & n \leq \frac{30}{dl} \\ 35 + 0.034(n-1)dl, & \frac{30}{dl} < n \leq \frac{H}{dl} \end{cases} \quad (21)$$

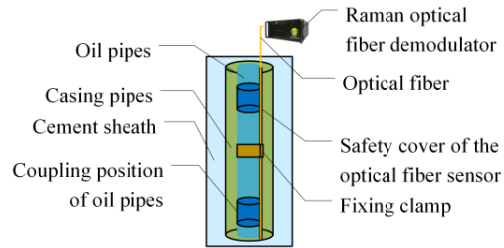


Figure 6. Schematic of Raman optical fiber temperature monitoring system

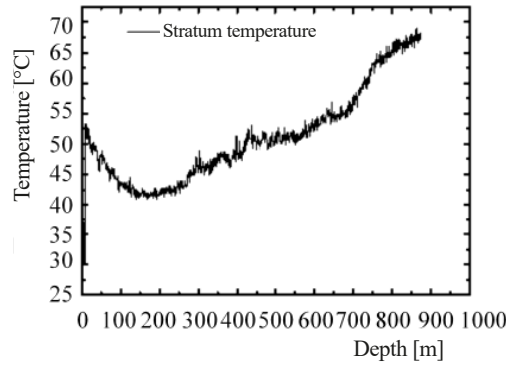


Figure 7. Distribution of temperature along axial direction

In the oil-field heat washover, the distribution of temperature in thermal washing process is monitored online through the Raman optical fiber temperature monitoring system. Temperature curves at different times are shown in fig. 8(a). Reducing the amount of extracted liquid obtains the temperature curves shown in fig. 8(b), the effective depth increases slightly with this reduction.

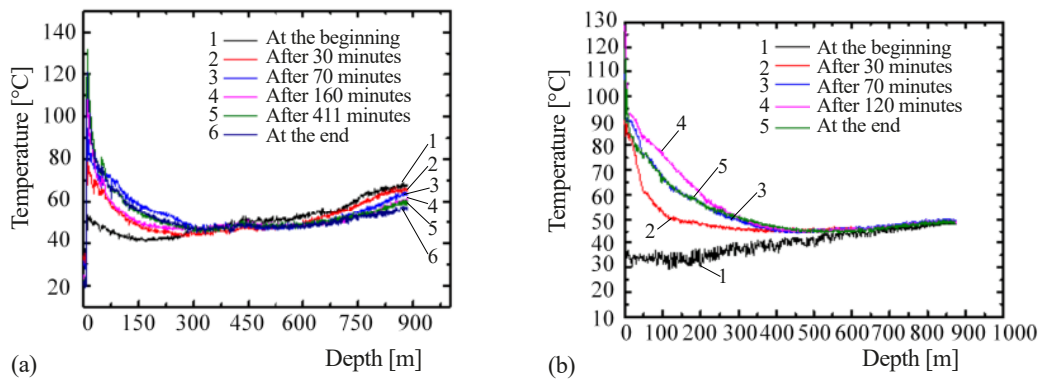


Figure 8. Data of superconducting car thermal washing; (a) Distributed curve in normal condition, (b) Distributed curve with parameter changes

Determination of optimal initial parameters in superconducting car thermal washing

Verification of accuracy of heat flow coupling model

To verify the accuracy of the heat flow coupling model, the theoretical temperature curve is established based on the heat flow coupling model and the real-time temperature curve based on the Raman optical fiber temperature monitoring system in the superconducting car thermal wash.

Based on the initial condition of superconducting car thermal wash at a certain test well, the initial condition of the heat flow coupling model is $d_l = 0.5$ m, $c = 4205$ J/kg $^{\circ}$ C, $H = 880$ m, $k_w = 5$ W/m $^{\circ}$ C, $k_t = 18.5$ W/m $^{\circ}$ C, $r_{to} = 0.0365$ m, $r_{ti} = 0.031$ m, $r_{ci} = 0.062$ m, $\rho = 0.997 \cdot 10^3$ kg/m 3 , $r_s = 0.115$ m, $q_i = 55$ m 3 /h, $T_{\alpha 0} = 110$ $^{\circ}$ C, $T_0 = 35$ $^{\circ}$ C, $\lambda = 0.034$ $^{\circ}$ C/m, $q_e = 32$ m 3 /d, and $t = 2.5$ h.

The theoretical temperature curve and the real time temperature curve of the tubing-casing annular space are shown in fig. 9. Comparing the two curves reveals that the great-

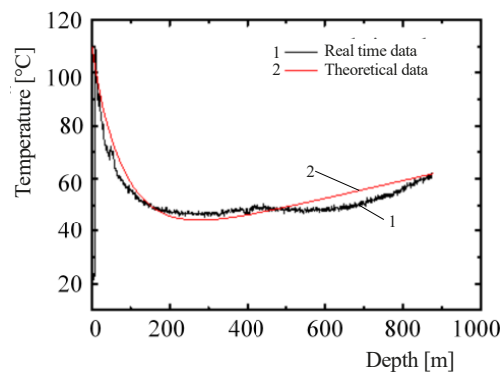


Figure 9. Contrast diagram of real time and theoretical data

est temperature deviation between them is approximately 5 $^{\circ}$ C at the depth of about 660 m. Thus, the heat flow coupling model in the oil-field heat washover is accurate and reliable and can be used to determine the optimal initial parameters.

Determination of optimal initial parameters through heat flow coupling model

Focused on superconducting car thermal washing, the changes of the effective depth are observed by changing the inlet liquid temperature, $T_{\alpha 0}$, liquid injection rate, q_i , liquid extraction rate, q_e , and cost of time, t , through the heat flow coupling model. The initial parameters are the same as those presented in the preceding section, and the melting point of petroleum wax is 55 $^{\circ}$ C.

- When other parameters remain unchanged and inlet liquid temperature, $T_{\alpha 0}$, is altered, the change of the effective depth with the inlet liquid temperature is obtained via the heat flow coupling model, as shown in tab. 4.

Table 4. Relation between effective depth and inlet liquid temperature

| | | | |
|--|-----|-----|-----|
| Inlet liquid temperature [$^{\circ}$ C] | 108 | 110 | 112 |
| Effective depth [m] | 115 | 117 | 120 |

not be too high, other parameters should be changed when inlet liquid temperature is increased to further enhance effective depth.

- When other parameters remain unchanged and the cost of time, t , is altered, the change of effective depth with the cost of time is obtained via the heat flow coupling model, as shown in tab. 5.

According to tab. 4, effective depth increases slightly with the rise of inlet liquid temperature. Because the temperature of the thermal washing liquid in superconducting car thermal washing can-

Table 5 shows that the effective depth of the thermal wash significantly increases as the thermal washing time is prolonged. When the thermal wash time is set to 7.5 h, the thermal wash effective depth reaches 334 m. The increase in the cost of time improves the effectiveness of paraffin removal and thermal efficiency. Thus, the cost of time should be set at 7.5 h.

- When other parameters remain unchanged and liquid injection rate, q_i , is altered, the change of the effective depth with the injection rate is obtained through the heat flow coupling model, as shown in tab. 6.

Table 6 shows that the effective depth increases with the increase in injection rate. When the injection rate is 65 m³/h, the effective depth is approximately 140 m, and the effectiveness of paraffin removal is improved. Thus, the liquid injection rate should be increased within the capacity of the thermal wash device.

- When other parameters remain unchanged and liquid extraction rate, q_e , is altered, the change of the effective depth with the liquid extraction rate is obtained via the heat flow coupling model, as shown in tab. 7.

Table 7 shows that the liquid extraction rate does not have a significant influence on the effective depth. Therefore, increasing the effective depth by changing the liquid extraction rate is not feasible, and other parameters need to be changed to increase effective depth.

Through the preceding analysis that involves changing different kinds of parameters, the present study proves that achieving good paraffin removal effectiveness by independently changing the thermal washing parameters is difficult. Therefore, only by changing various thermal washing parameters at the same time can the ideal effectiveness of paraffin removal be realized.

After the parameters are adjusted many times, a set of optimal parameters are obtained through the heat flow coupling model. When inlet liquid temperature is 110 °C, injection rate is 60 m³/h, extraction rate is 32 m³/h, and cost of time is 7.5 h, the effective depth of the thermal wash reaches 368 m, which results in very good effectiveness of thermal paraffin removal. This set of parameters should be used in the superconducting car thermal washing at the test wells and is able to increase the effective depth of the thermal wash and improve the effectiveness of thermal paraffin removal and the efficiency of the thermal wash.

After the parameters are adjusted many times, a set of optimal parameters are obtained through the heat flow coupling model. When inlet liquid temperature is 110 °C, injection rate is 60 m³/h, extraction rate is 32 m³/h, and cost of time is 7.5 h, the effective depth of the thermal wash reaches 368 m, which results in very good effectiveness of thermal paraffin removal. This set of parameters should be used in the superconducting car thermal washing at the test wells and is able to increase the effective depth of the thermal wash and improve the effectiveness of thermal paraffin removal and the efficiency of the thermal wash.

Conclusion

This study proposes a heat flow coupling model to theoretically analyze the temperature of tubing-casing annular space along the axial direction and to ultimately improve the negative effect of thermal washing caused by the difficulty of adjusting parameters in superconducting car thermal washing process. Using the superconducting car thermal washing process at the test oil well in Daqing as the research object, several sets of temperature with different initial conditions are obtained through the Raman optical fiber temperature monitoring system. Compared with the real-time data, theoretical data exhibit a maximum deviation of 5 °C; this

Table 5. Relation between effective depth and cost of time

| | | | |
|---------------------|-----|-----|-----|
| Cost of time [h] | 2.5 | 5 | 7.5 |
| Effective depth [m] | 117 | 229 | 334 |

Table 6. Relation between effective depth and injection rate

| | | | |
|--|-----|-----|-----|
| Injection rate [m ³ h ⁻¹] | 55 | 60 | 65 |
| Effective depth [m] | 117 | 129 | 140 |

Table 7. Relation between effective depth and liquid extraction rate

| | | | |
|--|-----|-----|-----|
| Liquid extraction rate [m ³ d ⁻¹] | 25 | 32 | 40 |
| Effective depth [m] | 117 | 117 | 117 |

amount of deviation verifies the accuracy of the heat flow coupling model. Based on the heat flow coupling model, this study investigates the influence of initial parameters on the effective depth. The effective depth increases with the increasing of inlet liquid temperature, the cost of time, and liquid injection rate, whereas the liquid extraction rate does not have an obvious influence on the effective depth. After several adjustments, the following set of optimal parameters is obtained: $T_{\alpha 0} = 110\text{ }^{\circ}\text{C}$, $t = 7.5\text{ h}$, $q_i = 60\text{ m}^3/\text{h}$, $q_e = 32\text{ m}^3/\text{d}$, and the effective depth reaches 368 m. Thus, determining the optimal parameters of different oil wells using this model is possible; these optimal parameters can increase the effective depth, improve the effectiveness of paraffin removal and thermal efficiency, prolong the maintenance period of pumps, and ultimately increase oil production. This study provides theoretical support and an inspection method to promote superconducting car thermal washing and paraffin removal and to improve productive efficiency.

Acknowledgment

This study is partially supported by the National Natural Science Foundation of China (grant 51074059), the National Natural Science Foundation of China (grant 61203358), and the Natural Science Foundation of Heilongjiang Province (grant F2015034).

References

- [1] Hosseinipour, A., *et al.*, The Impact of the Composition of the Crude Oils on the Wax Crystallization, *Proceedings, Applied Mechanics and Materials*, 3rd International Conference on Process Engineering and Advanced Materials., Kuala Lumpur, Malaysia, 2014, Vol. 625, pp. 196-200
- [2] Valinejad, R., Nazar, A. R. S., An Experimental Design Approach for Investigating the Effects of Operating Factors on the Wax Deposition in Pipelines, *Fuel*, 106 (2013), 2, pp. 843-850
- [3] Zhang, F., *et al.*, Potential Microorganisms for Prevention of Paraffin Precipitation in a Hypersaline Oil Reservoir, *Energy Fuels*, 28 (2014), 2, pp. 1191-1197
- [4] Zhang, F., *et al.*, Paraffin Deposition Mechanism and Paraffin Inhibition Technology for High-Carbon Paraffin Crude Oil from the Kazakhstan PK Oilfield, *Petroleum Science and Technology*, 32 (2014), 4, pp. 488-496
- [5] He, Y. W., Technical Research for Oil Well Variable Frequency Electromagnetic Field Paraffin Prevention, *Proceedings, Applied Mechanics and Materials*, 4th International Conference on Applied Mechanics, Materials and Manufacturing., Shenzhen, China, 2014, Vol. 670, pp. 313-317
- [6] Wang, W., *et al.*, Experimental Study on Mechanisms of Wax Removal during Pipeline Pigging, *Proceedings, Society of Petroleum Engineers, SPE Annual Technical Conference and Exhibition.*, Houston, Tex., USA, 2015
- [7] Danilović, D. S., *et al.*, Solving Paraffin Deposition Problem in Tubing by Heating Cable Application, *Thermal Science*, 14 (2010), 1, pp. 247-253
- [8] Hasan, A. R., *et al.*, Wellbore Heat-Transfer Modeling and Applications, *Journal of Petroleum Science and Engineering*, 86 (2012), 3, pp. 127-136
- [9] Izgec, B., Transient Fluid and Heat Flow Modeling in Coupled Wellbore/Reservoir Systems, *Spe Reservoir Evaluation and Engineering*, 10 (2007), 3, pp. 294-301
- [10] Fang, M., Research on Temperature Sensor System and Temperature Resolution Enhancement of Distributed Raman Optical Fiber (in Chinese), M. Sc. thesis, University of Electronic Science and Technology, Chengdu, China, 2004
- [11] Cheng, G., Study of Heat Fluid Coupling during the Process of Circulation of Warm Liquid and Temperature Monitoring System (in Chinese), M. Sc. thesis, Harbin Institute of Technology, Harbin, China, 2011
- [12] He, J., Research on Some Key Technologies of Distributed Fiber Sensing System (in Chinese), Ph. D. thesis, Harbin Institute of Technology, Harbin, China, 2010